Energy 149 (2018) 979–989

Contents lists available at ScienceDirect

Energy

journal homepage: www.elsevier.com/locate/energy

Effects of injection timing and injection pressure on performance and exhaust emissions of a common rail diesel engine fueled by various concentrations of fish-oil biodiesel blends

Jiaqiang E [a, c], MinhHieu Pham [a, b, c, **], Yuanwang Deng [a, c, *], Tuannghia Nguyen [b, ***], VinhNguyen Duy [d, ****], DucHieu Le [a, b], Wei Zuo [a, c], Qingguo Peng [a, c], Zhiqing Zhang [a, c]

[a] State Key Laboratory of Advanced Design and Manufacturing for Vehicle Body, Hunan University, Changsha 410082, China
[b] Faculty of Automobile Technology, Hanoi University of Industry, Hanoi City 10000, Viet nam
[c] Institute of New Energy and Energy-saving & Emission-reduction Technology, Hunan University, Changsha 410082, China
[d] Department of Internal Combustion Engine, School of Transportation Engineering, Hanoi University of Science and Technology, Hanoi City 10000, Viet Nam

ARTICLE INFO

Article history:
Received 24 April 2017
Received in revised form
10 February 2018
Accepted 12 February 2018
Available online 13 February 2018

Keywords:
Diesel engine
Varying fish oil proportion
Exhaust emission
Biodiesel
Injection timing
Pressure injection

ABSTRACT

To evaluate the performance and emissions of a test engine fueled by biodiesel blends produced from fish processing by-products, the experimental and simulation methods were used to investigate the effects of injection pressure and timing on engine operation and correlation of these effects with varying fish-oil concentrations in the biodiesel blends. Consequently, commercial diesel fuel blended with different concentrations of fish-oil biodiesel including B0, B10, B20, B30, B40 and B50 (corresponding to 0%, 10%, 20%, 30%, 40%, and 50% of biodiesel in blend) were used for the test engine. Compared to B0, the average reduction in brake power of the biodiesel fuels was reduced proportionally with the biodiesel ratio in the fuel blends. The brake specific fuel consumption (BSFC) and NO_x emissions increased together with a reduction in soot, HC and CO emissions as the percentage of biodiesel increases. Moreover, the engine characteristics depend on operating parameters such as injection timing and injection pressure as also mentioned in many previous studies. When increasing injection timing, the brake power initially increases until reaching a maximum value and then decreases slightly for all types of fuels tested. Meanwhile, the effect of injection pressure differs depending on the pressure range and biodiesel blends.

1. Introduction

In recent years, the energy consumption demand [1,2] and the polluted environment [3–5] have increased rapidly throughout the world. To solve these problems, it is necessary to find new energy sources to replace traditional energy sources [6,7]. As for alternative energy sources such as biomass, wind, solar and geothermal, biodiesel is considered a potential renewable energy source [8–11] since it can be supplied effectively [12–14] and provides sustainable development to solve these problems [15–17]. Moreover, with the abundance of raw materials (agricultural waste, animal fats, waste oil, algae) [18,19], a biodiesel development plan is a good solution to motivate farmers to participate in sustainable agriculture in developing countries [20,21].

Vietnam, a developing country in Southeast Asia [22], has a tropical monsoon climate with a long coastline, which has abundant resources for seafood production; therefore, it is convenient for seafood breeding, exploitation, processing and export. According to reports, the catfish industry in Vietnam exports more than 1.2 million tons per year [23]. However, the current practice of fish processing generates large quantities of by-products, which reaches 75% of the total fish weight. Despite the presence of some useful components, the by-products are usually dumped into landfills, which causes potentially harmful environmental effects,

* Corresponding author. State Key Laboratory of Advanced Design and Manufacturing for Vehicle Body, Hunan University, Changsha 410082, China.
** Corresponding author. Faculty of Automobile Technology, Hanoi University of Industry, Hanoi city 10000, Vietnam.
*** Corresponding author.
**** Corresponding author.
E-mail addresses: minhhieu186@gmail.com (M. Pham), dengyuanwang610@126.com (Y. Deng), tuannghiaoto@gmail.com (T. Nguyen), vinh.nguyenduy@hust.edu.vn (V. Duy).

https://doi.org/10.1016/j.energy.2018.02.053
0360-5442/

or appear as low-commercial value products. Consequently, fish processing by-products [24] can be considered an alternative raw material for the preparation of high-protein ingredients, especially since they are a reliable source of raw material for biodiesel production.

As shown in much of the literature, biodiesel and their blends were used in diesel engines, and their emissions and performance characterizations have been investigated [25]. For instance, Lu et al. [26] experimentally investigated the influence of waste cooking oil-derived biodiesel on diesel engine characteristics. The authors studied a 4-cylinder diesel engine using a range of biodiesel blends such as B5, B20 and B30. The results of this research showed that, compared with the use of pure diesel fuel, those biodiesel blends did not improve engine performance; however, their emission characteristics were dramatically improved. In another study, Godiganur et al. [27] determined the effect of blend ratio of mahua oil in biodiesel on engine performance and emission. They showed that with a higher mahua oil ratio in the blend, lower HC and CO emissions and higher brake specific fuel consumption (BSFC) and higher NO_x emission were achieved. Other studies [28–31] have reported that, compared to using fossil diesel fuel, using biodiesel as engine fuel leads to higher BSFC and NO_x emissions. Rao et al. [32] used rice bran oil biodiesel for their experimental research and determined that soot was reduced when biodiesel was used to operate the engine. Lešnik et al. [33,34] used the experimental and numerical method to investigate combustion, performance and emission characteristics of the diesel, biodiesel and their blends in a heavy-duty DI diesel engine and the influence of biodiesel fuel on injection characteristics, diesel engine performance and emission formation. And the results showed that neat biodiesel or biodiesel-diesel blends can be fueled for a heavy-duty diesel engine when the static fuel delivery angle of the mechanically-controlled injection system had been modified. Iclodean and Burnete [35] studied the processes occurring during operation of a single cylinder compression ignition engine with direct injection, fueled by biofuels, the results revealed that the NO_x content of exhaust gases can be reduced by setting some optimal load, engine speed and combustion gas recirculation.

In diesel engine operation, engine emission and performance characteristics are affected significantly by operating parameters such as injection timing and injection pressure [36]. Optimum injection timing primarily depends on the engine torque, engine speed, injection pressure, injection duration, and fuel properties, as shown in Refs. [37–41]. Concerning injection timing research, Bari and Lin [42] conducted experimental research on the effect of fuel injection timing with waste cooking oil (WCO) as a fuel in a direct injection engine. The tests were performed at rated speed, various engine loads and different injection timing. The results showed that optimum injection timing for the shortest ignition delay occurred at an earlier time for WCO. Banapurmath et al. [43] compared the effects of different injection of pressure (IOP) on engine performance for Honge oil methyl ester. They reported an improvement in the brake thermal efficiency (BTE) for biodiesel and that the highest BTE for the IOPs tested was 260 bar due to atomization, evaporation, and the fuel-air mixture being better with higher injection, which led to more perfect combustion. In another work, Jindal et al. [44] investigated the effect of the engine design parameters, compression ratio and injection pressure, on the performance and emission characteristics of a diesel engine fuelled with Jatropha methyl ester diesel fuel. They selected three injection pressures such as 150, 200, and 250 bar for their study. The results showed that at an injection pressure of 250 bar, BTE is improved by 8.9%, with reduced HC and smoke compared to the base injection pressure. The compression ratio is also an important parameter affecting the performance, emission and combustion characteristics [45,46]. Raheman et al. [45] studied the effect of compression ratio and injection timing on the performance and emissions of a Ricardo E6 engine using biodiesel obtained from mahua oil (B100) and its blend. They reported that increasing the compression ratio improved the efficiency of the engine. When the compression ratio was increased from 18 to 20, the mean BTE of the Ricardo engine increased by more than 33%, which may be due to the reduced ignition delay.

This paper presents a simulation and experimental study to investigate the impact of injection timing, injection pressure and biodiesel blends with varying fish oil proportions on the performance and emission characteristics of a common rail diesel engine. Consequently, the engine performance and emissions of the test engine fuelled by biodiesel blends were compared with those of standard diesel fuel by both simulation and experiment. They were performed at various engine speeds and high-load conditions using AVL Boost software and an engine dynamometer test bed. Corresponding to each type of fuel, the injection timing and injection pressure are also conducted to evaluate their effect on the test engine operation. The main aim of this work is to produce renewable, clean, low-cost raw materials and environmentally friendly fuels that meet the requirements of Vietnam. In addition, optimization of the engine operating parameters was also conducted to improve the engine characteristics with different blends of biodiesel fuel.

2. Simulation procedure

In this research, the simulation model was built based on structures of the test engine using AVL Boost software. Theoretical backgrounds including the basic equations and calculation models for all components of the model are clearly described in Ref. [47].

2.1. Basic conservation equations

The calculation of the high-pressure cycle of an internal combustion engine is based on the first law of thermodynamics as given in Eq. (1) and Eq. (2).

$$\frac{\mathrm{d}(m_c \cdot u)}{\mathrm{d}\alpha} = -p_c \cdot \frac{\mathrm{d}V}{\mathrm{d}\alpha} + \frac{\mathrm{d}Q_F}{\mathrm{d}\alpha} - \sum \frac{\mathrm{d}Q_W}{\mathrm{d}\alpha} - h_{BB} \cdot \frac{\mathrm{d}m_{BB}}{\mathrm{d}\alpha} \tag{1}$$

$$\frac{\mathrm{d}m_c}{\mathrm{d}\alpha} = \sum \frac{\mathrm{d}m_i}{\mathrm{d}\alpha} - \sum \frac{\mathrm{d}m_e}{\mathrm{d}\alpha} - \sum \frac{\mathrm{d}m_{BB}}{\mathrm{d}\alpha} + \sum \frac{\mathrm{d}m_{ev}}{\mathrm{d}t} \tag{2}$$

where m_c is the mass in the cylinder; u is the specific internal energy; p_c is the cylinder pressure; V is the cylinder volume; Q_F is the fuel energy; Q_W is the wall heat loss; α is the crank angle; h_{BB} is the enthalpy of blow-by; m_{BB} is the blow-by mass flow; d_{mi} is the mass element flowing into the cylinder; d_{me} is the mass element flowing out of the cylinder and m_{ev} is the mass of evaporating fuel.

This means that the change in internal energy in the cylinder is equal to the sum of the piston work, fuel heat input, wall heat losses and enthalpy flow due to blow-by. Eq. (1) is valid for engines with internal and external mixture preparation. However, the terms, which the change of the gas composition due to combustion is considered, are treated differently for internal and external mixture preparation. For internal mixture preparation in a diesel engine, the assumptions are made as follows: (1) the fuel added to the cylinder charge is immediately combusted; and (2) the combustion products mix instantaneously with the remaining cylinder charge and form a uniform mixture and the A/F ratio of the charge diminishes continuously from a high value at the start of combustion to the final value at the end of combustion. Consequently, Eq. (1) is transformed as follows:

$$\frac{dT_c}{d\alpha} = \frac{1}{m_c\left(\frac{\partial u}{\partial T} + \frac{\partial u}{\partial p}\cdot\frac{p_c}{T_c}\right)}\left[\frac{dQ_F}{d\alpha}\left(1 - \frac{S_c}{H_c}\right) - \frac{dQ_W}{d\alpha} - \frac{dm_{BB}}{d\alpha}(h_{BB} - S_c) - m_c\frac{\partial u}{\partial \lambda}\cdot\frac{\partial \lambda}{\partial \alpha} - p_c\frac{dV_c}{d\alpha}\left(1 - \frac{\partial u}{\partial p}\cdot\frac{m_c}{V_c}\right)\right] \quad (3)$$

where T_c is the gas temperature in the cylinder; H_c is the lower heating value, $S_c = u_c + p_c(\partial u/\partial p)$; and λ is the air–fuel equivalence ratio.

To solve this equation, models for the combustion process and the wall heat transfer, as well as the gas properties as a function of pressure, temperature, and gas composition, are required. Establishing the relation between pressure, temperature and density, Eq. (1) for the in-cylinder temperature can be solved by using of the Runge-Kutta method. Once the cylinder temperature is known, the cylinder pressure can be obtained from the gas equation.

2.2. Combustion model

BOOST uses the AVL MCC (Mixture Controlled Combustion) model to predict the combustion characteristics and the rate of heat release in direct injection compression ignition engines. The model requires the number of injector holes, the hole diameter, the discharge coefficient of the injector holes and the rail pressure to calculate the effective hole area, velocity and kinetic energy of the fuel jet. By shortening the ignition delay due to developments in recent years, the causal and time-related connection between injection and combustion has become very close. Therefore, the heat release is controlled by the fuel quantity available and the turbulent kinetic energy density:

$$\frac{dQ}{d\phi} = C_{Mod}\cdot f_1(M_F, Q)\cdot f_2(k, V) \quad (4)$$

where

$$f_1(M_F, Q) = M_F - \frac{Q}{LCV} \quad (5)$$

$$f_2(k, V) = \exp\left(C_{Rate}\cdot\frac{\sqrt{k}}{\sqrt[3]{V}}\right) \quad (6)$$

where C_{Mod} is the model constant; C is the mixing rate constant; k is the local density of turbulent kinetic energy; M_F is the injected fuel mass; LCV is the lower heating value; Q is the cumulative heat release; V is the instantaneous cylinder volume; and φ is the crank angle.

Since the distributions of squish and swirl to the kinetic energy are relatively small, only the kinetic energy input from the fuel spray is considered [47]. The amount of kinetic energy imparted to the cylinder charge is determined by the injection rate using.

2.3. Heat transfer model

The heat transferred to the walls of the combustion chamber is calculated by Eq. (7).

$$Q_{wi} = A_i\cdot\alpha_i\cdot(T_c - T_{wi}) \quad (7)$$

where Q_{wi} is the wall heat flow; A_i is the surface area; α_i is the heat-transfer coefficient; and T_{wi} is the wall temperature.

The heat-transfer coefficient (α_i) is usually calculated using the Woschni model, which was published in 1978 for high-pressure cycles, and is summarized as follows:

$$\alpha_w = 130D^{-0.2}\cdot p_c^{0.8}\cdot T_c^{-0.53}\left[C_1\cdot c_m + C_2\frac{V_D\cdot T_{c1}}{p_{c,1}\cdot V_{c,1}}\left(p_c - p_{c,0}\right)\right]^{0.8} \quad (8)$$

where $C_1 = 2.28 + 0.308\ (c_u/c_m)$; $C_2 = 0.00324$ for direct-injection engines, D is the cylinder bore, c_m is the mean piston speed, c_u is the circumferential velocity, V_D is the displacement per cylinder, $p_{c,o}$ is the cylinder pressure of the motored engine (bar), $T_{c,1}$ is the temperature in the cylinder at the intake valve closing (IVC), and $p_{c,1}$ is the pressure in the cylinder.

2.4. Test engine model

The test engine used in this research is a single-cylinder, four-stroke, common rail diesel engine, named AVL 5402. The engine specifications and engine modelled by AVL Boost software are shown in Fig. 1.

3. Experimental procedure

3.1. Test engine and fuel characteristics

The engine used in this study, AVL-5402, is a naturally aspirated, single-cylinder, four-stroke, direct injection diesel engine, named AVL-5402. Table 1 shows a diagram and some main technical parameters of the engine. The test engine uses the common rail fuel system and the open-ECU. The injection process is controlled using INCA, which is a programme that allows the user to set and control the parameters of injection such as injection timing, injection pressure, and injection duration.

3.2. Test fuels

In this study, the test fuels are a fossil diesel fuel in the Vietnam market and a biodiesel blend of fossil diesel fuel and fish oil. The fatty acid composition of the biodiesel was evaluated at an early stationary growth phase and its characteristics are shown in Table 2. Some physico-chemical properties of the test fuels corresponding to B0, B10, B20, B30, B40, B50, and B100 are shown in Table 3 and correspond to the ASTM measurement standard. B100 fuel is 100% pure biodiesel. B10, B20, B30, B40 and B50 have 10%, 20%, 30%, 40% and 50% volume percentages of B100.

As shown in Table 3, the heating values of B10, B20, and B30 are similar to B0 but are significantly different from B100. In addition, all other parameters of biodiesel blends are greater than B0 fuel.

3.3. Test equipment

Fig.2 shows a schematic diagram of the experimental apparatus.

AC motor/generator dynamometer: The AMK, produced in Germany, was used in the experiment to load the engine. The dynamometer can operate in either motor or generator mode. Some technical specifications of the AMK are as follows: maximum power, torque, and speed of 28 kW, 150 Nm, and 7000 rpm, respectively. The AMK parameters are described in Table 4.

Emission analysis system: Carbon monoxide (CO), nitrogen oxides (NO_x), and un-burnt hydrocarbon (UBHC) emissions are collected and analysed with an AVL Combustion Emission Bench (CEBII). The CEBII combines the analysers for HC, CO, and NO_x measurements. CO emissions are analysed using Non-Dispersive Infrared (NDIR) analysers, while the HC emission analyser uses a Flame Ionization Detector (FID), and NO_x emissions are analysed

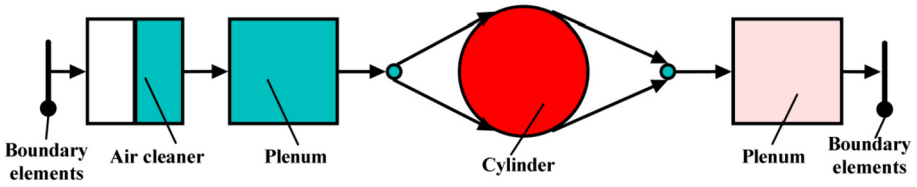

Fig. 1. Diesel engine AVL 5402 model.

with a Chemiluminescence Detector (CLD). Each analyser has 4 measurement ranges that can be automatically adjusted to align with measured values to increase accuracy.

EMCON 300 (Engine and Dyno Controller) is a complete digital test bed control and monitoring system for a combustion engine and a dynamometer on an engine test bed. FEM (Modular Data Acquisition) is a modular data acquisition system for measurement tasks for in-vehicle testing as well as on the test bed.

Opacimeter (smoke measurement unit): An AVL 415S smoke metre is used to measure the smoke number of the diesel engine. The device determines the opacity of the diesel engine smoke using a filter. The black level of the filter after the exhaust current passes through is converted to the smoke result. The measurements range from 0 to 9.99 FSN (Filter Smoke Number) or from 0 to 31999 mg/m^3 with a 0.1% deviation.

Fuel balance: The quantity of fuel consumed by the vehicle is measured with fuel-consumption measurement equipment, the Fuel Balance AVL 733S, using the gravimetrical method. The fuel system enables high-precision fuel-consumption measurements, even at low consumption and short measuring times. The measuring range of the equipment is up to 150 kg/h with an accuracy of 0.12%. The parameters of the Fuel Balance AVL 733S are shown in Table 5.

3.4. Experimental setup of the test engine

In this research, the test engine was operated at engine speeds ranging from 1200 rpm to 3000 rpm. Based on the test engine characteristics, the brake specific fuel consumption (BSFC) is lowest at an engine speed of 2200 rpm and engine load of 75%. In the experimental process, the mode of the lowest BSFC was selected for the comparison. Consequently, the engine speed and engine load position were maintained for the entire experimental process at a moderate value of 2200 rpm and 75% load, respectively. Corresponding to each type of fuel, injection timing was varied from 12° before top dead centre (BTDC) to 22° BTDC at an interval of 2° to evaluate the influence of its variation. In addition, the injection pressure was varied from 400 bar to 800 bar at an interval of 100 bar. Consequently, the brake mean effective power, brake specific fuel consumption, and exhaust emissions, such as NO_x, UBHC, CO, and smoke number, were measured, recorded, and analysed.

Table 2
Fatty acid profile of biodiesel used in this research.

Fame	Fame composition (%)
$C_{14}H_{28}O_2$ (Tetradecanoic)	4.70
$C_{16}H_{32}O_2$ (Hexadecanoic)	34.20
$C_{16}H_{30}O_2$ (9-Hexadecenoic)	1.18
$C_{18}H_{36}O_2$ (Octadecanoic)	10.60
$C_{18}H_{34}O_2$ (9- Octadecenoic)	40.05
$C_{18}H_{32}O_2$ (9-12-Octadecadienoic)	6.65

4. Result and discussion

4.1. Comparison of engine performance and fuel consumption

To validate the simulation model, the simulation and experimental results are compared. Fig. 3 shows a comparison of the power and fuel consumption between the simulation and experiments using B0, B10, B20, and B30. The largest power deviation, 6% (between the simulation and experiment), is observed with B0, and the smallest power deviation, 2.61%, is observed with B30. Meanwhile, the largest and smallest deviation of BSFC is 5.05% with B0 and 4.77% with B30. In addition, the mean deviation values between the simulation and experiment for B0, B10, B20, B30 fuels are 6.00%, 5.71%, 5.10%, and 4.76%, respectively, and the mean fuel consumption values are 5.77%; 5.19%; 4.52% and 4.33%, respectively. Slight variation between the simulated and experimental data can be attributed to the assumptions used in the simulation process. However, these assumptions can not be controlled in the experiments. In addition, many important operational and physicochemical parameters of the simulation models are difficult to reproduce in the actual values. However, the simulated results are

Table 1
Technical specifications of the test engine.

Item	Technical parameters	Unit
Name of engine	**AVL-5402**	
Type of engine	Diesel, 4 strokes; Naturally aspirated	
Number of cylinders	1	
Bore x Stroke	85 × 90	mm
Connecting rod length	148	mm
Crank radius	45.0	mm
Displacement	510.7	cm^3
Max. power/engine speed	18/4200	kW/rpm
Max. torque/engine speed	29.3/1400	N·m/rpm
Lubricating system	Dry pump	–
Cooling system	Closed circuit	
Combustion system	Direct injection	
Injection nozzle type	Common Rail CP1 type (5 holes nozzle)	
Compression ratio	17.3:1	

Table 3
Comparison of biodiesel blend and diesel fuel properties.

Property	B0	B10	B20	B30	B40	B50	B100	ASTM
Heating value (MJ/kg)	42.76	42.26	41.84	41.29	41.03	40.68	37.58	D240
Cetane No.	49	50	51	52	53	54	56	D613
Density (kg/m^3)	838	840	845	848	852	857	866	D1298
Kinematic viscosity at 40 °C (mm^2/s)	3.22	3.31	3.47	3.56	3.67	3.76	4.4	D445
Flash point (°C)	67	71	75	80	84	89	142	D93
Sulfur (ppm)	428	430	433	436	439	441	26	D5453
Water content (ppm)	62	84	96	110	122	136	215	D6304

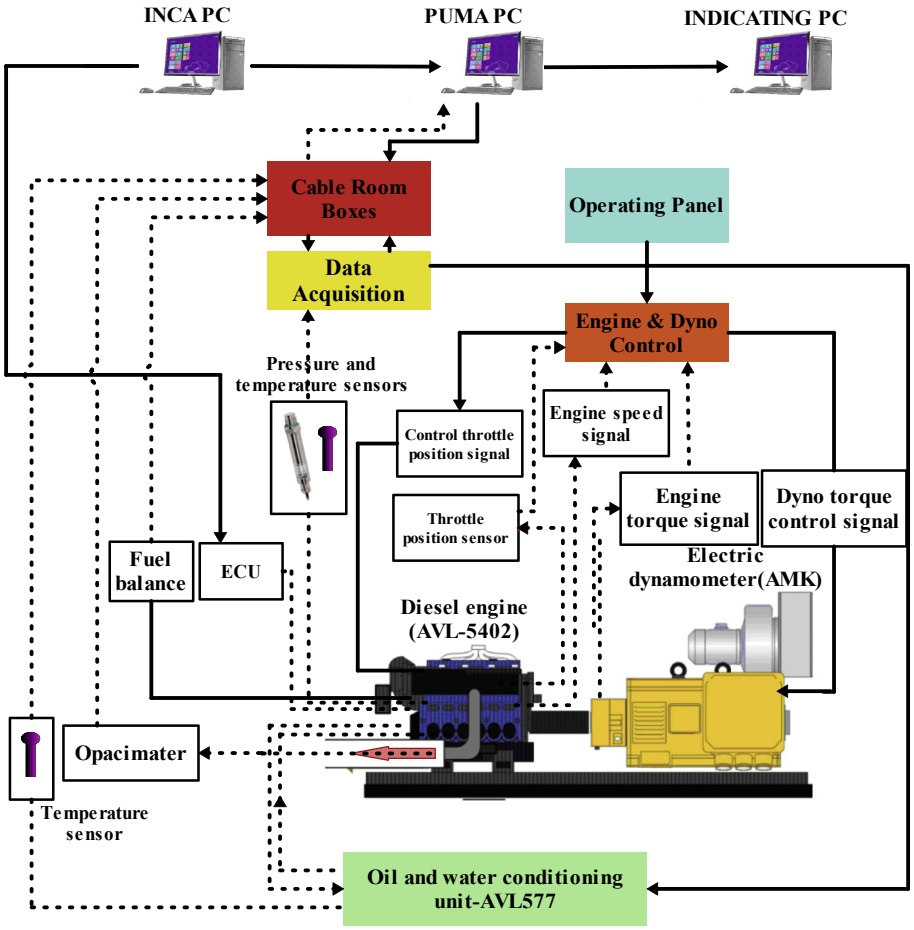

Fig. 2. Schematic diagram of the experimental setup.

Table 4
Technical specifications of the dynamometer.

Item	Technical parameters
Torque	180 N m from 0 to 3000 rpm
Power	60 kW from 3000 to 7950 rpm
Torque flange	500 N m
Supply voltage	3 × 400 V AC, PE, 50/60 Hz
Cooling water supply	~6 m^3/h at min. 3 bar
Weight	2.400 kg (with options, without Single Cylinder Engine)
Testing mode	steady state testing
Oil circuit: Temperature range	40 … 120 °C (±1 °C) p-max. 5 bar
Coolant circuit: Temperature range	50 … 110 °C (±1 °C) p-max. 1.4 bar

still useful for engine research and development.

In the simulation and experiment procedures of this research, the supplied amount of fuel for a cycle was constantly controlled for all the tested fuel blends. The results shown in Fig. 3 indicate that increasing the blend ratio of biodiesel reduces the brake power and increases fuel consumption. This is because increasing the biodiesel

Table 5
Technical specifications of the AVL fuel balance.

Item	Technical parameters
Recommended measuring range	0 … 150 kg/h (wider ranges up to 240 kg/h on request)
Vessel capacity	1800 g can be switched to 900 g/450 g/225 g
Systematic measurement uncertainty	Us = 0.12%
Maximum measurement frequency	10 Hz
No. of measurements (running average)	1 … 99
Ambient temperature	0 … 60 °C
Fuel temperature	−10 … +70 °C
Fuel supply pressure to the system	0.1 … 0.8 bar
Fuel supply flow	max. consumption +100 kg/h
Fuels	Otto (EN228), Diesel (EN590), up to 6% Biodiesel (EN14214) and 20% alcohol With Flex Fuel option: up to 100% alcohol and biodiesel
Interfaces	RS232 (AK compliant) or 733/730 protocol Analogue 0 … 10 V (optional) Digital I/0 (optional)
Power supply	24 V ± 0.5 VDC, 1.6 A
Power consumption	40 W
Dimensions	510 × 640 × 280 mm (W × H × D)
Weight (dry)	approx. 45 kg

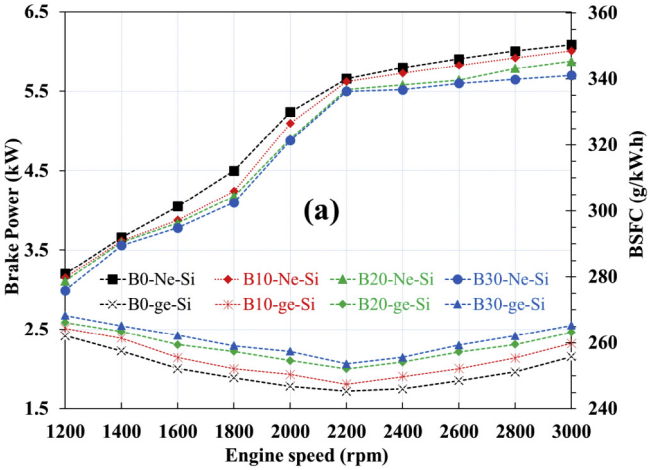

Simulated performance characteristics of the test engine fueled by different biodiesel concentrations. B0-Ne-Si, B10-Ne-Si, B20-Ne-Si, B30-Ne-Si and B0-ge-Si, B10-ge-Si, B20-Ne-Si, B30-ge-Si are the test engine powers and fuel consumptions corresponding to B0, B10, B20 and B30, respectively.

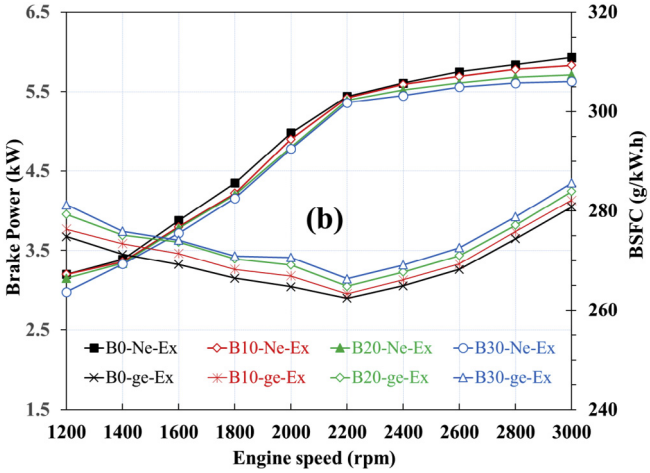

Experimental performance characteristics of the test engine fueled by different biodiesel concentrations. B0-Ne-Ex, B10-Ne-Ex, B20-Ne-Ex, B30-Ne-Ex and B0-ge-Ex, B10-ge-Ex, B20-ge-Ex, B30-ge-Ex are the test engine powers and fuel consumptions corresponding to B0, B10, B20 and B30, respectively.

Fig. 3. Comparison between simulation and experimental results of brake power and brake specific fuel consumption with B0, B10, B20 and B30 fuels.

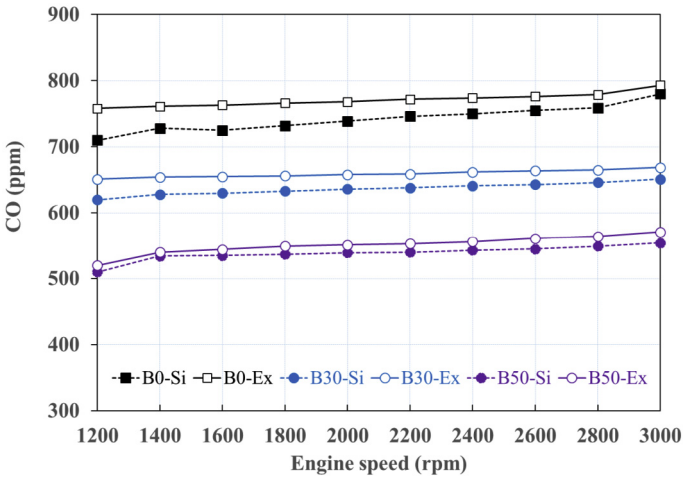

Simulation and experimental CO emissions characteristics of the test engine fueled by different biodiesel concentrations. B0-Si, B30-Si, B50-Si and B0-Ex, B30-Ex, B50-Ex are the test engine CO emissions corresponding to B0, B30 and B50, respectively

Fig. 4. Comparison between simulation and experimental results of CO emissions.

blending ratio reduces the lower heating value due to the characteristics of biodiesel, and the engine power is reduced. Moreover, the density and kinematic viscosity of the biodiesel blends also increase when the biodiesel blending ratio increases; this causes a reduction in evaporation ability, which leads to a decrease in the efficiency of combustion and increases fuel consumption.

4.2. Comparison of exhaust emission

As shown in the CO, smoke and NOx emission diagrams (Figs. 4, 5, 7 and 8), the absolute values in ppm are expressed, but the relative percentage difference between the simulated and experimental results of CO, NOx, and PM is approximately 8% in all three cases. As described in the literature, CO and HC emissions are the products of combustion due to the absence of oxygen. The addition of biodiesel into fossil diesel causes the increase of oxygen content of the blends, which improves the oxygen-to-fuel ratio in the fuel rich regions. This advantage of biodiesel overcomes the disadvantage related to the density and kinematic viscosity; consequently, combustion is more complete and CO and HC emissions are reduced. In this research, because the amount of supplied fuel per cycle was constantly controlled for all the fuels, the stoichiometry of biodiesel blends is greater than that of diesel fuel, which enhances the oxidation ability. When the engine speed is increased, the ignition delay and evaporation of fuel is reduced. Then, CO emissions are increased and HC emissions are reduced. This trend occurs for all the fuel blends tested, as shown in Figs. 4 and 5.

The mean deviation value of CO emission between the

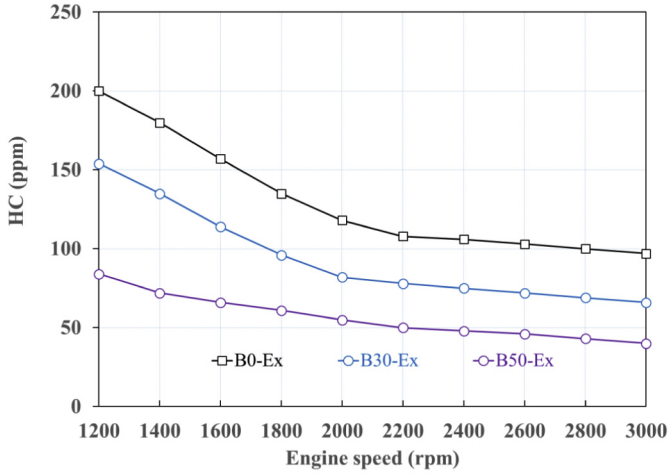

Experimental HC emissions characteristics of the test engine fueled by different biodiesel concentrations. B0-Ex, B30-Ex, B50-Ex are the test engine HC emissions corresponding to B0, B30 and B50, respectively

Fig. 5. Experimental results of HC emissions.

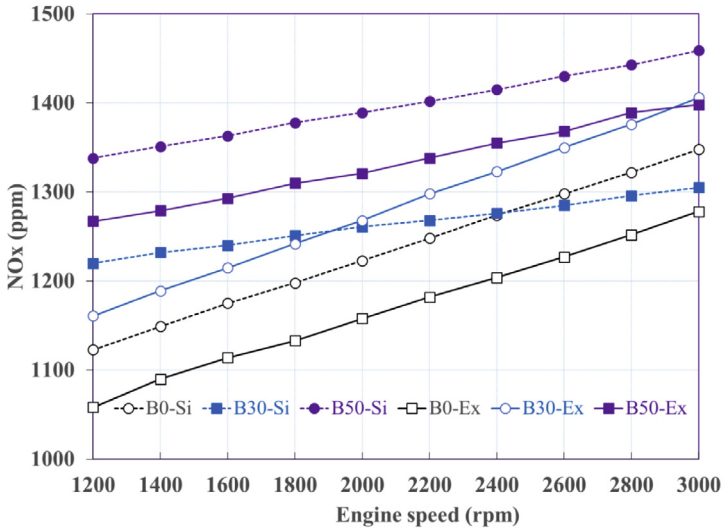

Simulation and experimental NOx emissions characteristics of the test engine fueled by different biodiesel concentrations. B0-Si, B30-Si, B50-Si and B0-Ex, B30-Ex, B50-Ex are the test engine NOx emissions corresponding to B0, B30 and B50, respectively

Fig. 6. Comparison between simulation and experimental results of NO_x emissions.

experimental and simulation results for B0, B30 and B50 is 3.37%, 3.19% and 3.23%, respectively. In this research, the commercial software AVL_BOOST was used for the simulation. This software uses the AVL MCC (Mixture Controlled Combustion) model to predict the combustion characteristics and rate of heat release in direct injection compression ignition engines [47]. Unfortunately, this combustion model ignores the formation of HC emissions due to the low formation as mentioned in which only shows the experimental results of HC emissions [48]. The HC emissions in the experiment follow the same trend of CO emissions described in Figs. 4 and 5.

Figs. 6 and 7 present the comparisons between the simulation and experimental results of NO_x and smoke emissions of B0, B30 and B50. As indicated by the CO, smoke and NO_x emission diagrams (Figs. 4, 6 and 7), the absolute values in ppm are expressed, but the relative percentage difference between the simulated and experimental tests of CO, NO_x, PM is approximately 8% in all three cases.

The mean deviation value of NO_x emission for B0, B30 and B50

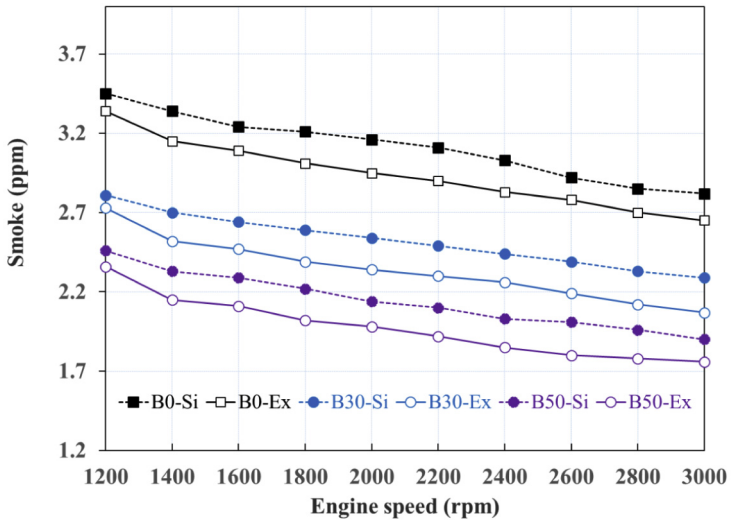

Simulated and experimental performance characteristics of the test engine fueled by different biodiesel concentrations. B0-Ne, B10-Ne, B20-Ne, B30-Ne, B40-Ne, B50-Ne and B0-ge, B10-ge, B20-ge, B30-ge, B40-ge, B50-ge are the test engine powers and fuel consumptions corresponding to B0, B10, B20, B30, B40 and B50, respectively

Fig. 7. Comparison between simulation and experimental results of Smoke emissions.

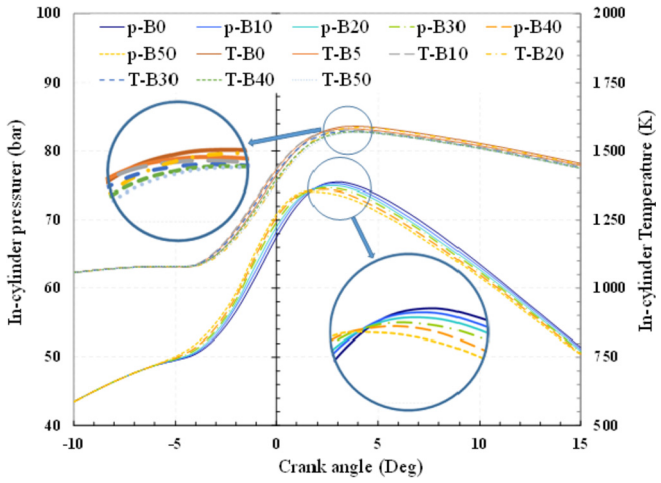

Fig. 8. Simulation comparison of temperature and pressure of the test engine fuelled by diesel and biodiesel blends.

fuels is 7.28%, 7.21% and 8.01%, respectively, and for smoke emissions, it is 7.24%, 6.87% and 8.2%, respectively. Additionally, it can be observed that NO_x emissions increased and smoke emissions decreased significantly as the biodiesel content increased. The reason for this phenomenon is that, compared to the stoichiometry of traditional diesel, the higher stoichiometry of biodiesel fuel blends leads to enhanced formation of NO_x emissions. On the other hand, the NO_x formation increased and smoke emissions decreased as the engine speed increases because the larger cetane number of biodiesel shortens the ignition delay. Therefore, the combustion process was enhanced resulting in an increased temperature, which contributes to the NO_x formation enhancement. As shown in Fig. 8, the in-cylinder temperature profiles among fuels are high and quite similar. Therefore, the oxygen content will have more influence on the different NO_x concentrations among the test fuels.

The higher oxygen content of biodiesel results in a more complete combustion process and further promotes the oxidation of soot. As the engine speed increases, the turbulence effect increases and the combustion efficiency improves and the extent of complete combustion is enhanced. As described in Ref. [47], CO, NOx, and soot formation are developed based on previous studies [49–51]. These formation emissions depend on the reaction rates, which can change due to system changes in concentration, pressure, or temperature caused by varying engine speeds. These emission models are validated at low engine speeds; as a result, there is good agreement between the simulated and experimental results, as shown in Figs. 4–7.

4.3. Effect of injection timing on engine characteristics

Brake power and brake specific fuel consumption of the engine using diesel and biodiesel fuel blends operating at a constant load and different injection timings are given in Fig. 8. When increasing the injection timing, the brake power initially increased until reaching a maximum value and then decreased slightly for all types of test fuels. The optimizational injection angle decreased corresponding to the increased biodiesel content, which means injection occurs later. The higher cetane number and increase of oxygen in biodiesel fuel blends contribute to earlier auto-ignition of the mixture, which means that the ignition delay can be shortened and the optimum injection angle is reduced. The higher kinematic viscosity also contributes to the advancing of the fuel injection, which causes the mixture to ignite earlier.

The results also show that the characteristic of BSFC is the same as brake power for every injection timing. Because the amount of fuel supplied per cycle is constantly controlled, BSFC reaches the minimum value when the brake power reaches the maximum value corresponding to the optimum injection angle. As a result, the

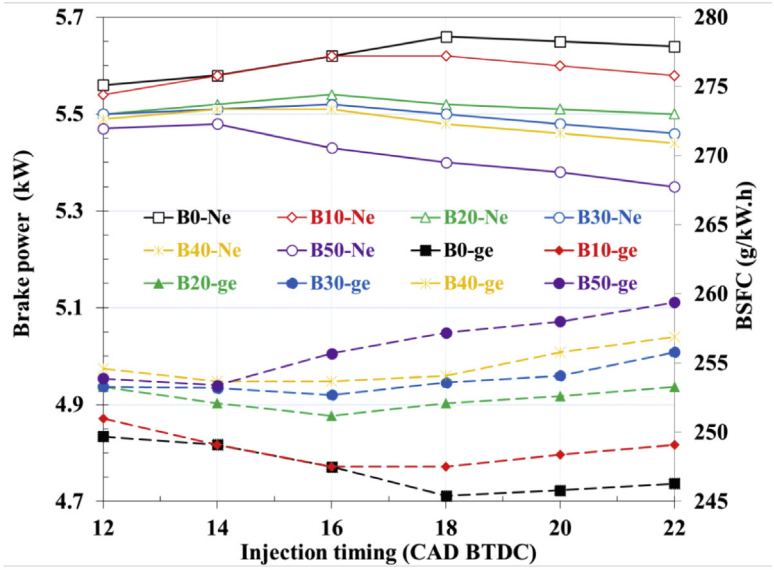

Simulated and experimental performance characteristics of the test engine fueled by different biodiesel concentrations. B0-Ne, B10-Ne, B20-Ne, B30-Ne, B40-Ne, B50-Ne and B0-ge, B10-ge, B20-ge, B30-ge, B40-ge, B50-ge are the test engine powers and fuel consumptions corresponding to B0, B10, B20, B30, B40 and B50, respectively

Fig. 9. Effect of injection timing on engine characteristics.

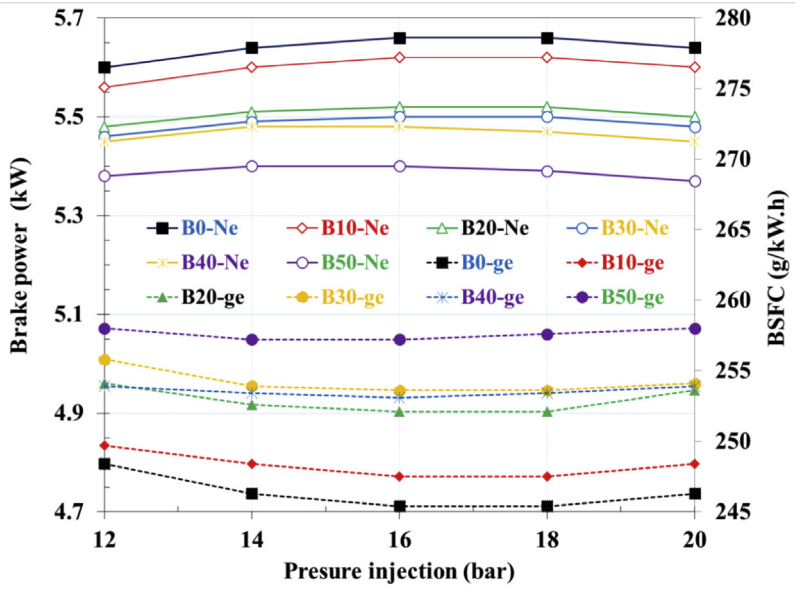

Simulated and experimental performance characteristics of the test engine fueled by different biodiesel concentrations. B0-Ne, B10-Ne, B20-Ne, B30-Ne, B40-Ne, B50-Ne and B0-ge, B10-ge, B20-ge, B30-ge, B40-ge, B50-ge are the test engine powers and fuel consumptions corresponding to B0, B10, B20, B30, B40 and B50, respectively

Fig. 10. Effect of injection pressure on engine characteristics.

optimum injection angle of BSFC is also the optimum injection angle of brake power.

4.4. Effect of injection pressure on engine characteristics

Fig. 10 shows the simulation results of brake power and BSFC for various injection pressures ranging from 400 bar to 900 bar corresponding to B0, B10, B20, B30, B40 and B50. When the injection pressure varies, the trend in brake power is the same for B0, B10, B20 and B30. Meanwhile, it is similar for B40 and B50. Accordingly, with B0, B10, B20 and B30, the brake power and BSFC do not vary in the pressure range from 600 bar to 700 bar. For this range of pressure, the brake power decreases and BSFC increases. However, for the B40 and B50 fuels, brake power and BSFC are the same at low injection pressures ranging from 500 bar to 600 bar; meanwhile, the brake power decreases and BSFC increases for this pressure range.

Fig. 9 also shows that the injection pressure has a greater effect on biodiesel blends than standard diesel since the viscosity of biodiesel is much greater than the viscosity of standard diesel. As a result, the pressure has more influence on the evaporation of the injected fuel mixing with the charged air. It shows that the adjusting injection pressure is unnecessary when using biodiesel fuel blends with a blend ratio less than 30%. However, when using biodiesel fuel blends with higher blend ratios, the injection pressure should be adjusted to enhance engine performance.

Compared with high injection pressure, low injection pressure leads to reduced spray characteristics and mixture with air, which results in an improved combustion process. When the injection pressure is greater than 900 bar, the spray characteristics are improved. However, the fuel injection process lasts longer; as a result, the collision and adhesion phenomena on the wall of the cylinder occur, and the combustion efficiency decreases. These reasons lead to decrease brake power and increase brake specific fuel consumption.

5. Conclusion

Biodiesel produced from seafood and agriculture products has been shown to be a sustainable energy source that provides energy requirements for transportation and reduced exhaust emissions. The results of this study show that the addition of biodiesel into fossil diesel causes the increase of oxygen content in the blends, which improves the oxygen-to-fuel ratio in the fuel-rich regions; consequently, combustion is more complete, and CO and HC emissions are reduced. Also, NO_x emissions are increased and smoke emissions are decreased significantly with the increased biodiesel content. This phenomenon occurs due to the higher stoichiometry of biodiesel fuel blends than those of traditional diesel causing enhanced formation of NOx emissions.

However, engine characteristics also depend on operating parameters including injection timing and injection pressure. Corresponding to the increase in biodiesel content, the optimum injection angle decreases while the time of injection occurs later. Meanwhile, the optimum pressure of the test engine depends on the biodiesel content of the fuel; for blending ratios of biodiesel in blends less than 30%, the adjusting injection pressure is unnecessary. Conversely, the research recommends the correction of injection pressure to enhance the engine characteristics.

Future research will focus on optimizing the operating engine parameters corresponding to each biodiesel blend to enhance the engine characteristics. In addition, observations of the combustion process of diesel engines and their modifications when using biodiesel blends will be made to fully understand engine operation.

Conflict of interests

The authors declare that they have no conflict of interests regarding the publication of this paper.

Acknowledgements

This work is supported by the National Natural Science Foundation of China under the research grant of 51676066.

References

[1] Deng Y, Liu H, Zhao X, E J, Chen J. Effects of cold start control strategy on cold start performance of the diesel engine based on a comprehensive preheat diesel engine model. Appl Energy 2018;210:279–87.
[2] E J, Zhang Z, Tu Z, Zuo W, Hu W, Han D, et al. Effect analysis on flow and boiling heat transfer performance of cooling water-jacket of bearing in the gasoline engine turbocharger. Appl Therm Eng 2018;130:754–66.
[3] Zhang B, E J, Gong J, Yuan W, Zuo W, Li Y, et al. Multidisciplinary design optimization of the diesel particulate filter in the composite regeneration process. Appl Energy 2016;181:14–28.
[4] E J, Zuo W, Gao J, Peng Q, Zhang Z, Pham M. Effect analysis on pressure drop of the continuous regeneration-diesel particulate filter based on NO_2 assisted regeneration. Appl Therm Eng 2016;100:356–66.
[5] E J, Han D, Deng Y, Zuo W, Qian C, Wu G, et al. Performance enhancement of a baffle-cut heat exchanger of exhaust gas recirculation. Appl Therm Eng 2018;134:86–94.
[6] Dincer I, Rosen MA. Thermodynamic aspects of renewables and sustainable development. Renew Sustain Energy Rev 2005;9(2):169–89.
[7] Bundschuh J, Chen G, Yusaf T, Chen S, Yan J. Sustainable energy and climate protection solutions in agriculture. Appl Energy 2014;114:735–6.
[8] Wen Z, Yu X, Tu ST, Yan J, Dahlquist E. Synthesis of biodiesel from vegetable oil with methanol catalyzed by Li-doped magnesium oxide catalysts. Appl Energy 2010;87(3):743–8.
[9] Cynthia OB, Lee KT, Lim JK. Comparative exergy analyses of Jatropha curcas oil extraction methods: solvent and mechanical extraction processes. Energy Convers Manag 2012;55:164–71.
[10] Lim S, Lee KT. Investigation of impurity tolerance and thermal stability for biodiesel production from Jatropha curcas L. seeds using supercritical reactive extraction. Energy 2014;68:71–9.
[11] Aghbashlo M, Demirbas A. Biodiesel: hopes and dreads. Biofuel Res J 2016;3(2). 379–379.
[12] Tabatabaei M, Karimi K, Horváth IS, Kumar R. Recent trends in biodiesel production. Biofuel Res J 2015;2:258–67.
[13] Sharma YC, Singh B, Madhu D, Liu Y, Yaakob Z. Fast synthesis of high quality biodiesel from 'waste fish oil' by single step transesterification. Biofuel Res J 2014;1:78–80.
[14] Kannan GR, Anand R. Effect of injection pressure and injection timing on DI diesel engine fuelled with biodiesel from waste cooking oil. Biomass bioenergy 2012;46:343–52.
[15] Hoekman SK, Robbins C. Review of the effects of biodiesel on NO_x emissions. Fuel Process Technol 2012;96:237–49.
[16] Enweremadu CC, Rutto HL. Combustion, emission and engine performance characteristics of used cooking oil biodiesel—A review. Renew Sustain Energy Rev 2010;14:2863–73.
[17] Khalife E, Tabatabaei M, Demirbas A, Aghbashlo M. Impacts of additives on performance and emission characteristics of diesel engines during steady state operation. Prog Energy Combust Sci 2017;59:32–78.
[18] Dias JM, Alvim-Ferraz MCM, Almeida MF, Díaz JDM, Polo MS, Utrilla JR. Biodiesel production using calcium manganese oxide as catalyst and different raw materials. Energy Convers Manag 2013;65:647–53.
[19] Rattanapoltee P, Kaewkannetra P. Cultivation of microalga, Chlorella vulgaris under different auto–hetero–mixo trophic growths as a raw material during biodiesel production and cost evaluation. Energy 2014;78:4–8.
[20] Piastrellini R, Arena AP, Civit B. Energy life-cycle analysis of soybean biodiesel: effects of tillage and water management. Energy 2017;126:13–20.
[21] Kuss VV, Kuss AV, Rosa RGD, Aranda DAG, Cruz YR. Potential of biodiesel production from palm oil at Brazilian Amazon. Renew Sustain Energy Rev 2015;50:1013–20.
[22] Tong YD. Rice intensive cropping and balanced cropping in the Mekong Delta, Vietnam — economic and ecological considerations. Ecol Econ 2017;132:205–12.
[23] Fisheries production in the first five months up 3.7 per cent. https://vpdt.tongcucthuysan.gov.vn/vietnam-fisheries/doc-tin/008109/2017-06-06/fisheries-production-in-the-first-five-months-up-37-per-cent, 05-06-2017.
[24] Bui TM, Phuong NT, Nguyen GH, Silva SSD. Fry and fingerling transportation in the striped catfish, Pangasianodon hypophthalmus, farming sector, Mekong Delta, Vietnam: a pivotal link in the production chain. Aquaculture 2013;388–391:70–5.
[25] E J, Pham M, Zhao D, Deng Y, Le D, Zuo W, et al. Effect of different technologies on combustion and emissions of the diesel engine fueled with biodiesel: a review. Renew Sustain Energy Rev 2017;80:620–47.
[26] Lu T, Cheung CS, Huang Z. Influence of waste cooking oil biodiesel on the particulate emissions and particle volatility of a DI diesel engine. Aerosol Air Qual Res 2013;13:243–54.
[27] Godiganur S, Murthy CHS, Reddy RP. 6BTA 5.9 G2-1 Cummins engine performance and emission tests using methyl ester mahua(Madhuca indica) oil/diesel blends. Renew Energy 2009;34:2172–7.
[28] Kalam MA, Masjuki HH. Emissions and deposit characteristics of a small diesel engine when operated on preheated crude palm oil. Biomass Bioenergy 2004;27:289–97.
[29] Ozsezen AN, Canakci M, Turkcan A, Sayin C. Performance and combustion characteristics of a DI diesel engine fueled with waste palm oil and canola oil methyl esters. Fuel 2009;88:629–36.
[30] Sanjid A, Masjuki HH, Kalam MA, Rahman SMA, Abedin MJ, Palash SM. Production of palm and jatropha based biodiesel and investigation of palm-jatropha combined blend properties, performance, exhaust emission and noise in an unmodified diesel engine. J Clean Prod 2014;65:295–303.
[31] E J, Liu T, Yang W, Deng Y, Gong J. A skeletal mechanism modeling on soot emission characteristics for biodiesel surrogates with varying fatty acid methyl esters proportion. Appl Energy 2016;181:322–31.
[32] Rao GLN, Prasad BD, Sampath S, Rajagopal K. Combustion analysis of diesel engine fueled with Jatropha oil methyl ester - diesel blends. Int J Green Energy 2007;4:645–58.
[33] Lešnik L, Iljaž J, Hribernik A, Kegl B. Numerical and experimental study of combustion, performance and emission characteristics of a heavy-duty DI diesel engine running on diesel, biodiesel and their blends. Energy Convers Manag 2014;81:534–46.
[34] Lešnik L, Vajda B, Žunic Z, Škerget L, Kegl B. The influence of biodiesel fuel on injection characteristics, diesel engine performance, and emission formation. Appl energy 2013;111:558–70.
[35] Iclodean C, Burnete N. Computer simulation of CI engines fuelled with biofuels by modelling injection iRate law. Res J Agric Sci 2012;44(1):249–57.
[36] Shameer PM, Ramesh K, Sakthivel R, Purnachandran R. Effects of fuel injection parameters on emission characteristics of diesel engines operating on various biodiesel: a review. Renew Sustain Energy Rev 2017;67:1267–81.
[37] Ganapathy T, Gakkhar RP, Murugesan K. Influence of injection timing on performance, combustion and emission characteristics of Jatropha biodiesel engine. Appl Energy 2011;88:4376–86.
[38] Ozsezen AN, Canakci M, Sayin C. Effects of biodiesel from used frying palm oil on the exhaust emissions of an indirect injection diesel engine. Energy Fuels 2008;22:2796–804.
[39] Liu T, E J, Yang W, Hui A, Cai H. Development of a skeletal mechanism for biodiesel blend surrogates with varying fatty acid methyl esters proportion. Appl Energy 2016;162:278–88.
[40] Zhang Z, E J, Deng Y, Zuo W, Peng Q, Hieu P, et al. Effects of fatty acid methyl esters proportion on combustion and emission characteristics of a biodiesel fueled marine diesel engine. Energy Convers Manag 2018;159:244–53.
[41] E J, Liu T, Yang WM, Li J, Gong J, Deng Y. Effects of fatty acid methyl esters proportion on combustion and emission characteristics of a biodiesel fueled diesel engine. Energy Convers Manag 2016;117:410–9.
[42] Bari S, Yu CW, Lim TH. Effect of fuel injection timing with waste cooking oil as a fuel in a direct injection diesel engine. Proc Inst Mech Eng 2004;218(1):93–104.
[43] Banapurmath NR, Tewari PG, Hosmath RS. Effect of biodiesel derived from Honge oil and its blends with diesel when directly injected at different injection pressures and injection timings in single-cylinder water-cooled compression ignition engine. Proc Inst Mech Eng Part A J Power Energy 2009;223(1):31–40.
[44] Jindal S, Nandwana BP, Rathore NS, Vashistha V. Experimental investigation of the effect of compression ratio and injection pressure in a direct injection diesel engine running on Jatropha methyl ester. Appl Therm Eng 2010;30:442–8.
[45] Raheman H, Ghadge SV. Performance of diesel engine with biodiesel at varying compression ratio and ignition timing. Fuel 2008;87:2659–66.
[46] Muralidharan K, Vasudevan D, Sheeba KN. Performance, emission and combustion characteristics of biodiesel fuelled variable compression ratio engine. Energy 2011;36:5385–93.
[47] AVL: Thermodynamic cycle simulation boost, Boost user's guide, Version 3.2.
[48] Liu H, Ma X, Li B, Chen L, Wang Z, Wang J. Combustion and emission characteristics of a direct injection diesel engine fueled with biodiesel and PODE/biodiesel fuel blends. Fuel 2017;209:62–8.
[49] Schubiger RA, Boulouchos K, Eberle MK. Rußbildung und Oxidation bei der dieselmotorischen Verbrennung. Mot Z 2002;63(5):342–53.
[50] Pattas K, Häfner G. Stickoxidbildung bei der ottomotorischen Verbrennung. Mot Z 1973;12:397–404.
[51] Onorati A, Ferrari G, D'Errico G. 1D unsteady flows with chemical reactions in the exhaust duct-system of S.I. Engines: predictions and experiments. SAE Paper No. 2001-01-0939. 2001.